npj | precision oncology

Article

Published in partnership with The Hormel Institute, University of Minnesota

https://doi.org/10.1038/s41698-026-01372-7

Integrated multi-omics analysis reveals that MARCKS reprograms the immunosuppressive microenvironment to drive hepatocellular carcinoma progression

Haifei Qin[1,2,3,5], Qinchen Lu[1,2,3,5], Baicheng Hu[1,2,3,5], Xin Zhou[1,2,3], Chenlu Lan[1,2,3], Honglong Lu[1,2,3], Donghua Gao[1,2,3], Chongjiu Qin[1,2,3], Kai Peng[1,2,3], Yongguang Wei[1,2,3], Xiwen Liao[1,2,3], Tao Peng[1,2,3] ✉, Liming Shang[4] ✉ & Guangzhi Zhu[1,2,3] ✉

Hepatocellular carcinoma (HCC) is one of the most lethal malignancies worldwide, and its progression is closely linked to the establishment of an immunosuppressive tumor microenvironment. Myristoylated alanine-rich C kinase substrate (MARCKS) has been implicated in tumor biology; however, its role in regulating immune interactions in HCC remains poorly defined. Here, we performed an integrated multi-omics analysis combining bulk transcriptomics, single-cell RNA sequencing, and spatial transcriptomics to systematically investigate the expression pattern and functional relevance of MARCKS in HCC. We found that MARCKS was significantly upregulated in HCC tissues and that high MARCKS expression was associated with aggressive clinicopathological features and unfavorable prognosis. Single-cell and spatial analyses revealed that MARCKS expression was enriched in myeloid cell populations within the tumor microenvironment. Functional annotation and mIF(Multiple immunofluorescence) validation demonstrated that MARCKS expression was associated with enhanced JAK/STAT3 signaling and M2-like macrophage polarization. Consistently, MARCKS silencing in HCC cell lines reduced STAT3 phosphorylation, suppressed malignant phenotypes in vitro, inhibited tumor growth in vivo, and diminished the capacity of tumor-derived conditioned media to promote macrophage M2 polarization. Together, these findings identify MARCKS as a key regulator of the immunosuppressive tumor microenvironment in HCC and highlight its potential as a therapeutic target for overcoming immune evasion.

Hepatocellular carcinoma is the most common primary liver malignancy and the third leading cause of cancer-related deaths worldwide[1]. Despite recent advances in surgical resection, targeted therapies, and immune checkpoint inhibitors, the prognosis of patients with advanced HCC remains dismal, primarily due to late-stage diagnosis, high recurrence rates, and therapeutic resistance[2–4]. Increasing evidence highlights the pivotal role of the tumor immune microenvironment (TIME) in shaping disease progression and determining therapeutic efficacy in HCC[5–8].

Among immune components, tumor-associated macrophages (TAMs) constitute one of the most abundant stromal populations and

[1]Department of Hepatobiliary Surgery, The First Affiliated Hospital of Guangxi Medical University, Nanning, PR China. [2]Guangxi Key Laboratory of Enhanced Recovery after Surgery for Gastrointestinal Cancer, Nanning, PR China. [3]Key Laboratory of Early Prevention & Treatment for Regional High Frequency Tumor (Guangxi Medical University), Ministry of Education, Nanning, PR China. [4]Department of Hepatobiliary Surgery, Beihai People's Hospital, Beihai, PR China. [5]These authors contributed equally: Haifei Qin, Qinchen Lu, Baicheng Hu.
✉e-mail: pengtaogmu@163.com; 231614649@qq.com; zhuguangzhi0792@hotmail.com

exhibit remarkable functional plasticity[9,10]. Classically activated (M1) macrophages exert antitumor effects by producing pro-inflammatory cytokines and enhancing immune surveillance[11]. In contrast, alternatively activated (M2) macrophages promote tumor progression by facilitating angiogenesis, tissue remodeling, and immunosuppression[12,13]. In HCC, the predominance of M2-polarized TAMs is strongly associated with poor clinical outcomes and resistance to immunotherapy[14,15]. However, the molecular mechanisms that drive TAM polarization and sustain the immunosuppressive niche remain incompletely understood.

Myristoylated alanine-rich C kinase substrate (MARCKS) is a well-established substrate of protein kinase C, involved in cytoskeletal dynamics, membrane trafficking, and intracellular signal transduction[16,17]. According to recent reports, aberrant expression of MARCKS has been implicated in peritoneal metastasis and tumor progression in gastric cancer, chemotherapy resistance in lung cancer, microsatellite instability and increased proliferation in colorectal cancer, as well as altered migration and motility in chronic lymphocytic leukemia (CLL) cells[18–22]. It is important to highlight that MARCKS plays a critical role in the initiation and progression of renal cancer. It not only promotes tumor growth and stimulates angiogenesis but also enhances resistance to various tyrosine kinase inhibitors[23].

Several lines of evidence further suggest that MARCKS may have important, yet underexplored, functions in HCC. Proteomic profiling studies have reported MARCKS as one of the proteins markedly overexpressed in HCC tissues compared with adjacent nontumorous liver, indicating its potential involvement in early hepatocarcinogenesis[24]. Other investigations examining pathological liver specimens revealed dynamic alterations in MARCKS expression and subcellular localization during the progression from chronic hepatitis to cirrhosis and finally to HCC, accompanied by enhanced phosphorylation and redistribution from the membrane to the cytosol, implying a role in hepatocyte transformation and malignant progression[25]. More recent genomic and transcriptomic analyses further confirm that MARCKS is significantly up-regulated in HCC, associated with higher tumor stage, vascular invasion, and unfavorable clinical outcomes. Importantly, MARCKS expression in HCC has been linked to dysregulated cell adhesion, ECM–receptor interaction, and proliferative signaling pathways[26]. Emerging evidence also indicates that MARCKS expression in tumor-associated macrophages correlates with immune cell infiltration patterns and may contribute to M2-like polarization and immune evasion[27]. Together, these findings suggest that MARCKS may participate not only in tumor-intrinsic malignant phenotypes but also in shaping the immunosuppressive microenvironment of HCC, warranting further mechanistic investigation.

In this study, we integrated bulk transcriptomic, single-cell, and spatial transcriptomic analyses to comprehensively evaluate the function of MARCKS in HCC. We show that MARCKS is significantly overexpressed in tumor tissues and correlates with adverse clinical features. At the single-cell level, MARCKS expression is enriched in myeloid populations, especially immunosuppressive TAMs. Spatial transcriptomic profiling and mIF further validate its colocalization with immunosuppressive macrophages in tumor regions. Functional assays demonstrate that MARCKS promotes malignant phenotypes of HCC cells while activating the JAK/STAT3 pathway, thereby driving M2 macrophage polarization and fostering an immunosuppressive TIME.

Collectively, our findings identify MARCKS as a critical regulator of macrophage polarization and immunosuppressive reprogramming in HCC, providing novel insights into its potential as both a prognostic biomarker and a therapeutic target.

Results

MARCKS is upregulated and clinically relevant in HCC

Pan-cancer analysis of TCGA and GTEx datasets revealed broad overexpression of MARCKS in multiple malignancies, including liver hepatocellular carcinoma (LIHC) (Fig. 1A). Within the TCGA-LIHC cohort, MARCKS was significantly higher in tumor tissues compared with normal counterparts. Clinically, MARCKS expression was positively associated with advanced pathological stage, higher histologic grade, elevated AFP, and vascular invasion (Fig. 1B). Details of the clinical data of the patients are listed in Table 1. Survival analyses demonstrated that high MARCKS predicted significantly worse overall survival (OS), disease-specific survival (DSS), and progression-free interval (PFI) (Fig. 1C). ROC analysis further supported its diagnostic potential (AUC = 0.785, Fig. 1D). Subgroup analyses confirmed increased MARCKS in aggressive subsets, including advanced stage, higher grade, AFP ≥ 400 ng/mL, and vascular invasion (Fig. 1E). Univariate and multivariate regression analyses confirmed that MARCKS was an independent prognostic risk factor for HCC (Table 2). The proportional hazards assumption for MARCKS was formally assessed using Schoenfeld residuals and showed no evidence of violation (Supplementary Table S1 and Supplementary Fig. S1A). In addition, a prognostic nomogram was constructed based on the multivariable Cox model, and its calibration for 1-, 3-, and 5-year survival probabilities was evaluated (Supplementary Fig. S1B–C).

Together, these findings establish MARCKS as a clinically relevant oncogene whose upregulation is associated with poor prognosis in HCC.

MARCKS correlates with immunosuppressive and pro-tumorigenic programs

Functional gene set analyses revealed enrichment of stemness, M2 macrophage polarization, immunosuppression, checkpoint signaling, and inflammation signatures in MARCKS-high tumors (Fig. 2A). Differential expression analysis identified multiple MARCKS-associated genes linked to tumor progression (Fig. 2B). Immune infiltration profiling demonstrated that MARCKS expression positively correlated with macrophages, Th2 cells, and NK subsets, while inversely correlating with Th17 cells (Fig. 2C). MARCKS also showed strong correlations with immunosuppressive checkpoint molecules (HAVCR2, CTLA4, PDCD1, LAG3) and cytokines (TGFB1, IL10, VEGFA, KLF4) (Fig. 2D, E). Co-expression networks further positioned MARCKS at the center of immunosuppressive and EMT-related hubs, including STAT6, CD274, MRC1, VIM, and ZEB1 (Fig. 2F).

These results indicate that MARCKS is intricately linked to immunosuppressive signaling and malignant phenotypes in HCC.

Distinct mutational landscapes stratified by MARCKS expression

Analysis of TCGA-LIHC mutation data revealed that 83.6% of patients harbored genetic alterations, with TP53, CTNNB1, and TTN being most frequent (Fig. 3A). Stratification by MARCKS expression uncovered distinct mutational landscapes: TP53 mutations were enriched in MARCKS-high tumors, whereas CTNNB1 mutations predominated in MARCKS-low tumors. Statistical analyses confirmed significant differences in mutation frequencies across several genes, including TP53, FLG, and PCLO (Fig. 3B).

These findings suggest that MARCKS expression defines HCC subgroups with distinct genomic backgrounds that may influence tumor biology and prognosis.

MARCKS is selectively enriched in myeloid populations in single-cell HCC

Single-cell transcriptomic analysis identified 22 clusters grouped into six major lineages: T/NK, B/Plasma, Myeloid, Endothelial, Hepatocyte, and Fibro/Stellate (Fig. 4A–C)(Markers for cell annotation are placed in Supplementary Table S2). MARCKS expression was selectively enriched in myeloid cells, with minimal expression in other immune or stromal lineages. UMAP feature plots and dot plots highlighted its lineage-specific localization (Fig. 4D–E), while violin plots revealed heterogeneity, with MARCKS concentrated in a subset of myeloid cells (Fig. 4F).

This myeloid-restricted expression pattern implicates MARCKS as a potential driver of macrophage polarization in HCC.

MARCKS defines an immunosuppressive TAM phenotype

Reclustering of myeloid cells identified functional subsets, including immunosuppressive TAMs, SPP1^{+} TAMs, dendritic cells, and monocytes

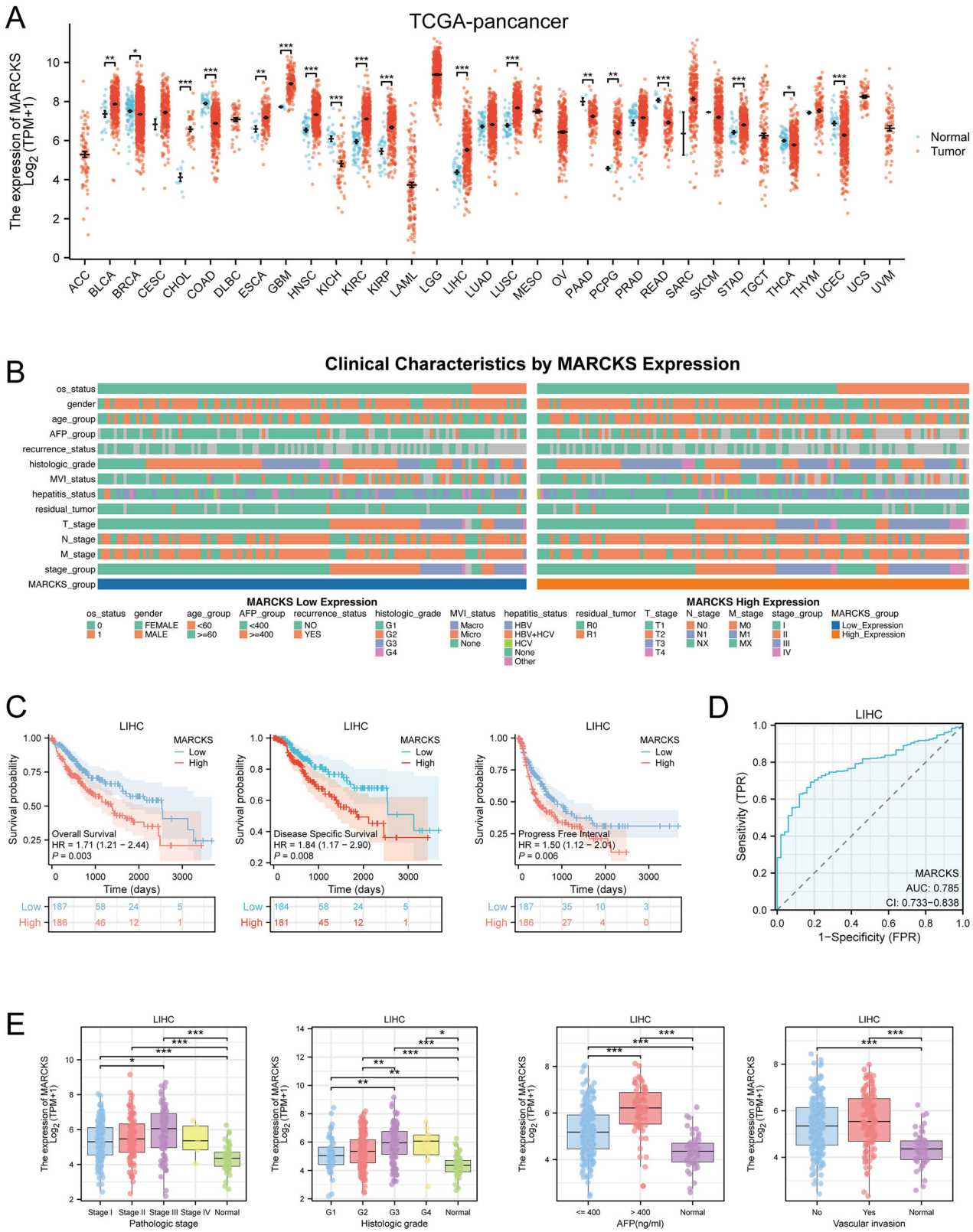

Fig. 1 | Expression and prognostic value of MARCKS in hepatocellular carcinoma. A Pan-cancer expression of MARCKS across TCGA and GTEx datasets. **B** Heatmap of clinicopathological characteristics stratified by MARCKS expression in TCGA-LIHC. **C** Kaplan–Meier curves for OS, DSS, and PFI. **D** ROC curve for diagnostic value (AUC = 0.785). **E** Subgroup analysis of MARCKS expression according to stage, grade, AFP, and vascular invasion.

(Fig. 5B, C). AUCell analysis demonstrated that MARCKS$^+$ myeloid cells scored significantly higher for M2 polarization, TREM2/SPP1 TAM, Differentiation and immunosuppression signatures compared with MARCKS$^-$ cells (Fig. 5A, G–H) (Gene sets used for this study are listed in Supplementary Table S3). UMAP visualization confirmed immunosuppressive TAMs as the predominant MARCKS$^+$ subset (Fig. 5D–F). Extreme subgroup analysis further emphasized distinct MARCKS$^+$/ImmHigh versus MARCKS$^-$/ImmLow populations (Fig. 5E).

Together, these results establish MARCKS as a molecular marker of immunosuppressive TAMs in HCC.

MARCKS associates with progenitor-like myeloid trajectories

CytoTRACE analysis revealed that immunosuppressive TAMs exhibited higher differentiation potential compared with other myeloid subsets, and MARCKS expression correlated positively with CytoTRACE scores (Fig. 6A). Trajectory reconstruction by Slingshot and Monocle2 delineated a progression from monocyte-like precursors toward immunosuppressive TAMs, with MARCKS expression increasing along pseudotime (Fig. 6B, C). Dynamic expression analyses demonstrated that MARCKS coincided with the upregulation of M2-associated and exhaustion-related genes such as CD163, MRC1, KLF4, and HAVCR2 (Fig. 6D, E).

These findings suggest that MARCKS is linked to progenitor-like myeloid states and contributes to their reprogramming into immunosuppressive TAMs.

MARCKS$^+$ myeloid cells are enriched for JAK/STAT3-mediated immunosuppressive signaling

Hallmark GSEA of MARCKS$^+$ myeloid cells demonstrated enrichment of immunoregulatory pathways, including IL6/JAK/STAT3, TNFα/NFκB, interferon responses, checkpoint pathways, and angiogenesis, whereas MYC targets were downregulated (Fig. 7A). KEGG enrichment in TCGA-LIHC tumors similarly confirmed activation of JAK–STAT signaling in MARCKS-high tumors (Fig. 7B).

These results highlight JAK/STAT3 signaling as a key mediator of MARCKS-driven immunosuppressive programming in HCC.

Cell–cell communication reinforces immunosuppression mediated by MARCKS$^+$ myeloid cells

CellChat analysis revealed that MARCKS$^+$ myeloid cells actively transmitted immunosuppressive signals such as VEGFA–VEGFR (angiogenesis), TNF–TNFR (inflammation), LGALS9–HAVCR2 (TIM-3), and MIF–(CD74 + CXCR4/CD44) (immune suppression) (Fig. 7C). As recipients, MARCKS$^+$ cells engaged in reciprocal signaling with immune and stromal cells, including MDK–SDC2 and MIF–(CD74 + CXCR4/CD44) (Fig. 7D).

These results suggest that MARCKS$^+$ myeloid cells function as central hubs of immunosuppressive communication within the HCC microenvironment.

Spatial colocalization of MARCKS$^+$ macrophages with immunosuppressive niches

Spatial transcriptomics revealed that MARCKS$^+$ macrophages were enriched in tumor regions compared with adjacent normal tissues (Fig. 8A). These cells colocalized with M2-score-high macrophages and overlapped extensively with immunosuppressive populations, including exhausted T cells, CAFs, MDSCs, tolerogenic DCs, and Tregs in tumor regions (Fig. 8B).

This spatial colocalization highlights a coordinated immunosuppressive niche centered on MARCKS$^+$ macrophages in HCC.

Experimental validation confirms MARCKS–STAT3 axis in HCC progression

Immunohistochemistry in the Guangxi cohort ($n = 34$) confirmed elevated MARCKS protein levels in tumors compared with adjacent tissues (Fig. 9A, B) (The clinical parameters of 34 patients are listed in Supplementary Table S4), consistent with HPA database validation (Fig. 9C). Multiplex immunofluorescence further showed colocalization of MARCKS with CD206$^+$ macrophages and PD-L1 (Fig. 9D), supporting its link to immunosuppressive macrophages.

In vitro, MARCKS knockdown or STAT3 inhibition by Stattic suppressed clonogenic growth, proliferation, migration, and invasion in HepG2 and Huh7 cells (Fig. 10A–C) (siRNA sequences used in this study are listed in Supplementary Table S5). Wound-healing assays demonstrated delayed closure in MARCKS-silenced or Stattic-treated cells (Fig. 11A). Western blotting confirmed efficient MARCKS knockdown and showed reduced STAT3 phosphorylation without affecting total STAT3 (Fig. 11B, C) (The original, uncropped western blot images corresponding to Fig. 11B, C are provided in Supplementary Fig. S2). Immunofluorescence further confirmed nuclear accumulation of p-STAT3 in MARCKS-expressing tumor tissues (Fig. 11D).

Table 1 | Baseline clinical characteristics of TCGA-LIHC patients stratified by MARCKS expression

Characteristics	Low expression of MARCKS	High expression of MARCKS	*P* value
n	187	187	
Pathologic T stage, *n* (%)			0.013
T1&T2	149 (40.2%)	129 (34.8%)	
T3&T4	36 (9.7%)	57 (15.4%)	
Pathologic N stage, *n* (%)			0.670
N0	123 (47.7%)	131 (50.8%)	
N1	1 (0.4%)	3 (1.2%)	
Pathologic M stage, *n* (%)			1.000
M0	134 (49.3%)	134 (49.3%)	
M1	2 (0.7%)	2 (0.7%)	
Pathologic stage, *n* (%)			0.007
Stage I & Stage II	141 (40.3%)	119 (34%)	
Stage III & Stage IV	34 (9.7%)	56 (16%)	
Tumor status, *n* (%)			0.030
Tumor free	112 (31.5%)	90 (25.4%)	
With tumor	67 (18.9%)	86 (24.2%)	
Gender, *n* (%)			0.320
Female	56 (15%)	65 (17.4%)	
Male	131 (35%)	122 (32.6%)	
Age, *n* (%)			0.004
<= 60	75 (20.1%)	102 (27.3%)	
>60	112 (30%)	84 (22.5%)	
BMI, *n* (%)			0.031
<= 25	81 (24%)	96 (28.5%)	
>25	92 (27.3%)	68 (20.2%)	
Histologic grade, *n* (%)			<0.001
G1&G2	137 (37.1%)	96 (26%)	
G3&G4	48 (13%)	88 (23.8%)	
Residual tumor, *n* (%)			0.123
R0	170 (49.3%)	157 (45.5%)	
R1&R2	6 (1.7%)	12 (3.5%)	
AFP(ng/ml), *n* (%)			<0.001
<= 400	137 (48.9%)	78 (27.9%)	
>400	14 (5%)	51 (18.2%)	
Child-Pugh grade, *n* (%)			0.980
A	130 (53.9%)	89 (36.9%)	
B&C	13 (5.4%)	9 (3.7%)	
Vascular invasion, *n* (%)			0.374
No	113 (35.5%)	95 (29.9%)	
Yes	54 (17%)	56 (17.6%)	

Table 2 | Univariate and multivariate Cox regression analyses of overall survival in TCGA-LIHC

Characteristics	Total(N)	Univariate analysis		Multivariate analysis	
		Hazard ratio (95% CI)	*P* value	Hazard ratio (95% CI)	*P* value
MARCKS	373				
Low	187	Reference		Reference	
High	186	1.714 (1.206–2.436)	**0.003**	1.626 (1.032–2.561)	**0.036**
Pathologic T stage	370				
T1&T2	277	Reference		Reference	
T3&T4	93	2.598 (1.826–3.697)	**<0.001**	2.456 (1.559–3.871)	**<0.001**
Pathologic N stage	258				
N0	254	Reference			
N1	4	2.029 (0.497–8.281)	0.324		
Pathologic M stage	272				
M0	268	Reference		Reference	
M1	4	4.077 (1.281–12.973)	**0.017**	1.244 (0.296–5.229)	0.766
Gender	373				
Female	121	Reference			
Male	252	0.793 (0.557–1.130)	0.200		
Child-Pugh grade	240				
A	218	Reference			
B&C	22	1.643 (0.811–3.330)	0.168		
Age	373				
<=60	177	Reference			
>60	196	1.205 (0.850–1.708)	0.295		
Vascular invasion	317				
No	208	Reference			
Yes	109	1.344 (0.887–2.035)	0.163		
AFP(ng/ml)	279				
<=400	215	Reference			
>400	64	1.075 (0.658–1.759)	0.772		
Tumor status	354				
Tumor free	202	Reference		Reference	
With tumor	152	2.317 (1.590–3.376)	**<0.001**	1.908 (1.195–3.047)	**0.007**
Histologic grade	368				
G1&G2	233	Reference			
G3&G4	135	1.091 (0.761–1.564)	0.636		
BMI	336				
<=25	177	Reference			
>25	159	0.798 (0.550–1.158)	0.235		
Residual tumor	344				
R0	326	Reference			
R1&R2	18	1.604 (0.812–3.169)	0.174		

Together, these findings validate that MARCKS promotes STAT3 activation and malignant phenotypes of HCC cells, thereby driving M2 macrophage polarization and shaping an immunosuppressive tumor microenvironment.

MARCKS knockdown suppresses tumor growth in vivo

To further evaluate the role of MARCKS in hepatocellular carcinoma progression in vivo, a subcutaneous xenograft tumor model was established using Huh7 cells. As shown in Fig. 12A, tumors derived from MARCKS-silenced cells exhibited significantly reduced growth compared with the control group. Consistently, longitudinal measurements revealed a significant reduction in tumor volume in the MARCKS knockdown group throughout the observation period (Fig. 12B). At the experimental endpoint, excised tumors from the MARCKS knockdown group were visibly smaller and displayed a significantly lower tumor weight than those from the control group (Fig. 12C). These results demonstrate that suppression of MARCKS inhibits tumor growth in vivo, supporting a pro-tumorigenic role of MARCKS in HCC.

MARCKS knockdown in HCC cells attenuates macrophage M2-like polarization via conditioned medium

To determine whether MARCKS expression in HCC cells influences macrophage polarization through tumor-derived soluble factors, a conditioned medium-based co-culture system using THP-1–derived

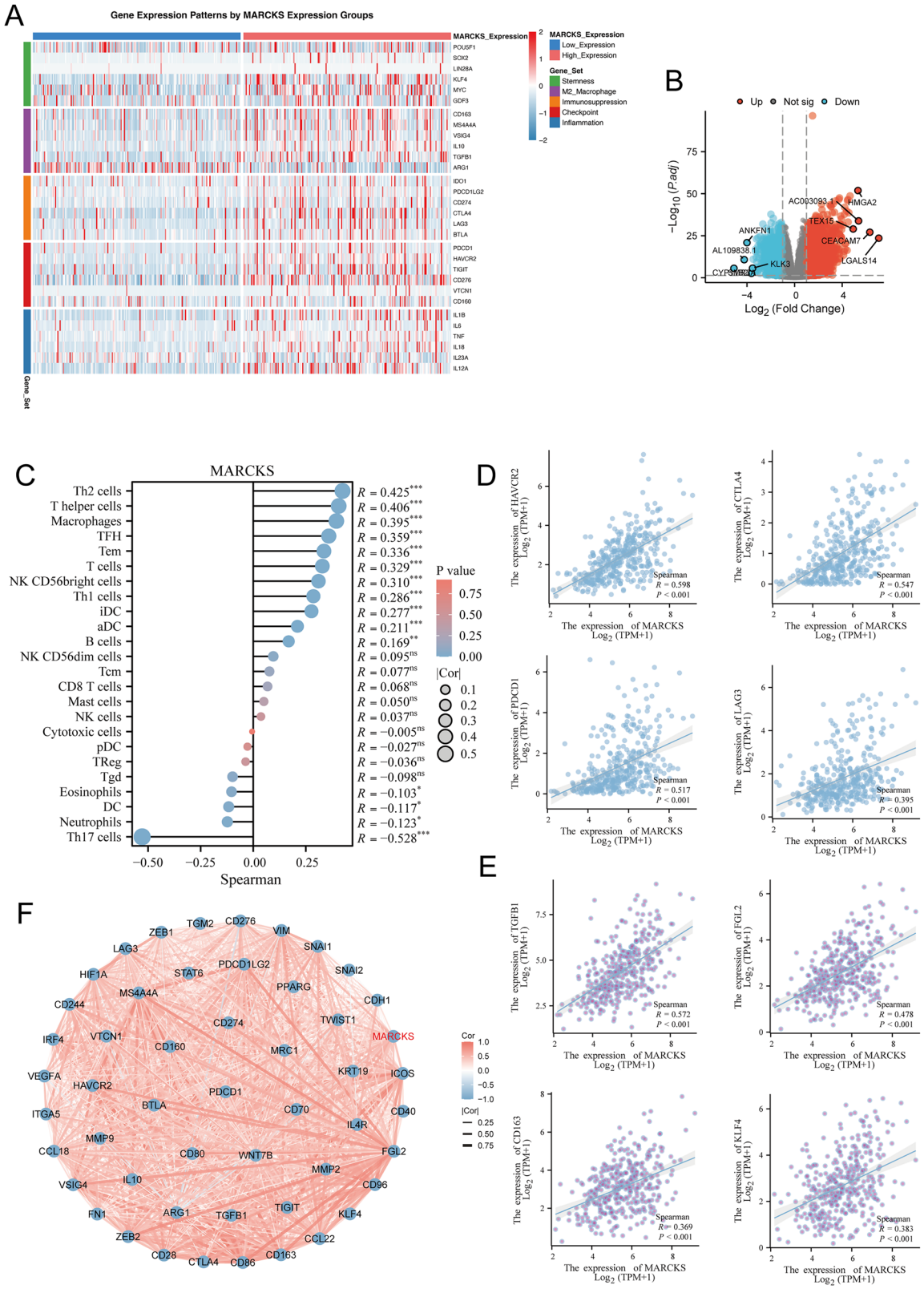

Fig. 2 | Functional associations of MARCKS in hepatocellular carcinoma. **A** Heatmap of functional gene sets (stemness, M2 macrophage, immunosuppression, checkpoint, inflammation) between MARCKS-high and MARCKS-low groups in TCGA-LIHC. **B** Volcano plot of differentially expressed genes (DEGs) associated with MARCKS expression. **C** Correlations between MARCKS expression and immune cell subsets estimated by xCell. **D** Spearman correlations between MARCKS expression and immune checkpoint genes (HAVCR2, CTLA4, PDCD1, LAG3). **E** Spearman correlations between MARCKS expression and immunosuppressive cytokines (TGFB1, IL10, VEGFA, KLF4). **F** Gene co-expression network showing MARCKS positively correlated with multiple immunosuppressive and EMT-related genes.

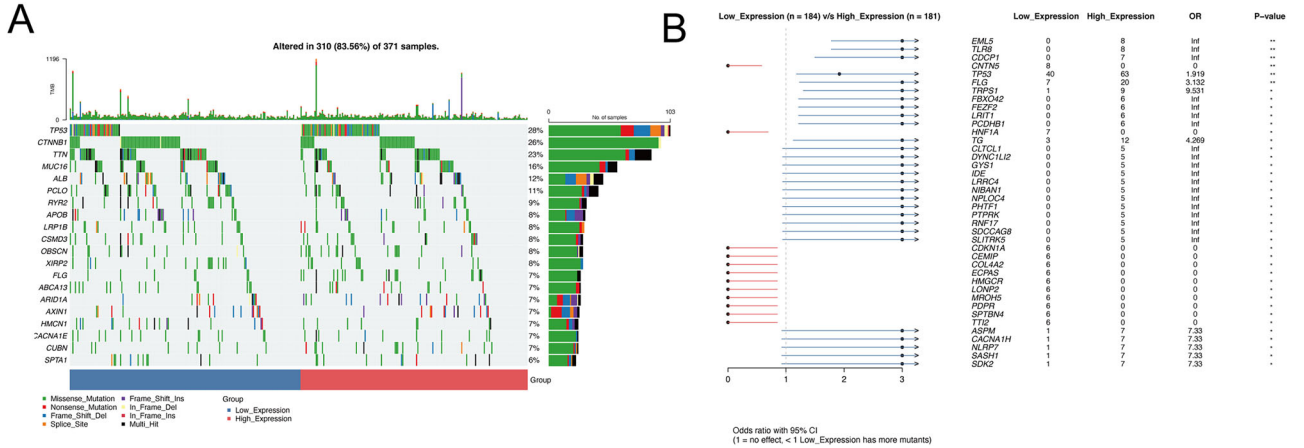

Fig. 3 | Somatic mutation landscape of MARCKS subgroups in TCGA-LIHC. **A** Mutation oncoplot showing the top 20 most frequently mutated genes in HCC, stratified by MARCKS-high and MARCKS-low expression groups. **B** Forest plot illustrating differentially mutated genes between MARCKS-high and MARCKS-low groups, with odds ratios (OR) and *p*-values indicated.

macrophages was established (Fig. 12D). Morphological observation showed that macrophages treated with conditioned medium from MARCKS-silenced HCC cells displayed altered morphology compared with those exposed to control conditioned medium (Fig. 12E).

Consistently, Western blot analysis revealed that conditioned media derived from MARCKS-knockdown Huh7 and HepG2 cells markedly reduced the expression of M2-associated markers, including CD163 and ARG1, in THP-1–derived macrophages, whereas the pan-macrophage marker CD68 remained relatively unchanged (Fig. 12F) (The original, uncropped Western blot images corresponding to Fig. 12F are provided in Supplementary Fig. S3).

Moreover, macrophages stimulated with conditioned medium from MARCKS-silenced HCC cells exhibited a pronounced decrease in STAT3 phosphorylation, while total STAT3 levels were largely unaffected (Fig. 12G)(The original, uncropped western blot images corresponding to Fig. 12G are provided in Supplementary Fig. S4). These findings indicate that suppression of MARCKS in tumor cells attenuates STAT3 activation in macrophages and impairs M2-like polarization.

Collectively, these results suggest that MARCKS expression in HCC cells promotes macrophage M2-like polarization, at least in part, through tumor-derived soluble factors, potentially via activation of STAT3 signaling.

Discussion

HCC remains a major health burden with high morbidity and mortality worldwide[28]. Despite recent advances in immune checkpoint inhibitors (ICIs), only a minority of patients derive durable benefit, and resistance remains a critical challenge[29–33]. TIME plays a decisive role in shaping response to immunotherapy[34–37], yet the molecular determinants that drive immunosuppression in HCC remain incompletely understood[38,39].

In this study, we identified MARCKS as a novel regulator of the immunosuppressive microenvironment in HCC. Comprehensive analyses integrating bulk, single-cell, and spatial transcriptomics demonstrated that MARCKS is highly expressed in HCC and preferentially enriched in myeloid subsets, particularly TAMs. MARCKS expression was strongly associated with signatures of M2 polarization and immune checkpoint activation. Spatial validation and mIF further confirmed colocalization of MARCKS with CD206 and PD-L1, providing direct evidence that MARCKS-expressing TAMs are embedded within immunosuppressive niches.

Our functional experiments revealed that siRNA-mediated knockdown of MARCKS in HCC cells significantly impaired proliferation, migration, and invasion, supporting its association with oncogenic phenotypes. Consistently, MARCKS silencing suppressed tumor growth in a subcutaneous xenograft model and attenuated STAT3 activation as well as M2-like macrophage polarization in macrophages exposed to tumor-derived conditioned media, providing functional evidence for a tumor cell-mediated immunoregulatory effect. Mechanistically, MARCKS suppression was accompanied by decreased phosphorylation of STAT3, a signaling event closely linked to macrophage polarization and immunoregulatory programs.

Immunofluorescence further demonstrated nuclear accumulation of p-STAT3 in MARCKS-expressing HCC tissues, supporting its role as a transcriptional driver of immune evasion programs. Together with enrichment analyses highlighting the JAK–STAT3 axis, these findings delineate a mechanistic pathway in which MARCKS promotes STAT3 activation, M2 macrophage polarization, and immune checkpoint upregulation, thereby contributing to the establishment of an immunosuppressive TIME.

These findings expand the functional spectrum of MARCKS beyond its canonical roles in cytoskeletal remodeling, motility, and metastasis. Previous studies have linked MARCKS overexpression to therapy resistance and poor outcomes in Lung cancer, multiple myeloma, hematological malignancies, glioma[22,40–43], but its immunological functions have remained largely unexplored. Our work is, to our knowledge, the first to implicate MARCKS in immune modulation in HCC. By linking MARCKS to STAT3 activation, we provide a novel mechanistic explanation for the enrichment of immunosuppressive TAMs and the limited efficacy of ICIs in HCC.

The clinical implications of our study are twofold. First, MARCKS may serve as a prognostic biomarker, as its high expression was associated with adverse pathological features and poor survival in TCGA-LIHC. Second, targeting MARCKS may represent a promising therapeutic strategy. Inhibition of MARCKS could remodel the immune landscape, reduce TAM-driven immunosuppression, and potentially sensitize tumors to ICIs. Moreover, the convergence of MARCKS signaling on STAT3 suggests that combinatorial strategies targeting the MARCKS–STAT3 axis could yield synergistic effects in overcoming ICI resistance.

Nonetheless, several limitations should be acknowledged. Our current data support a correlation and preliminary functional link between MARCKS expression and STAT3 activation, but do not establish a direct upstream regulatory mechanism, and macrophage-intrinsic roles of MARCKS were not directly interrogated. In vivo validation was limited to a subcutaneous xenograft model in nude mice, which does not allow assessment of immunotherapy synergy in an intact immune context; moreover, the single-cell and spatial analyses relied on public datasets without an independent in-house scRNA-seq/ST cohort. Future studies using macrophage-specific perturbation, orthotopic/immunocompetent models (including ICI-based evaluation), and in-house multi-omics cohorts will be important to strengthen mechanistic and translational conclusions.

In conclusion, our study uncovers a previously unappreciated role of MARCKS in shaping the immunosuppressive landscape of hepatocellular carcinoma. Beyond its established functions in tumor cell motility and

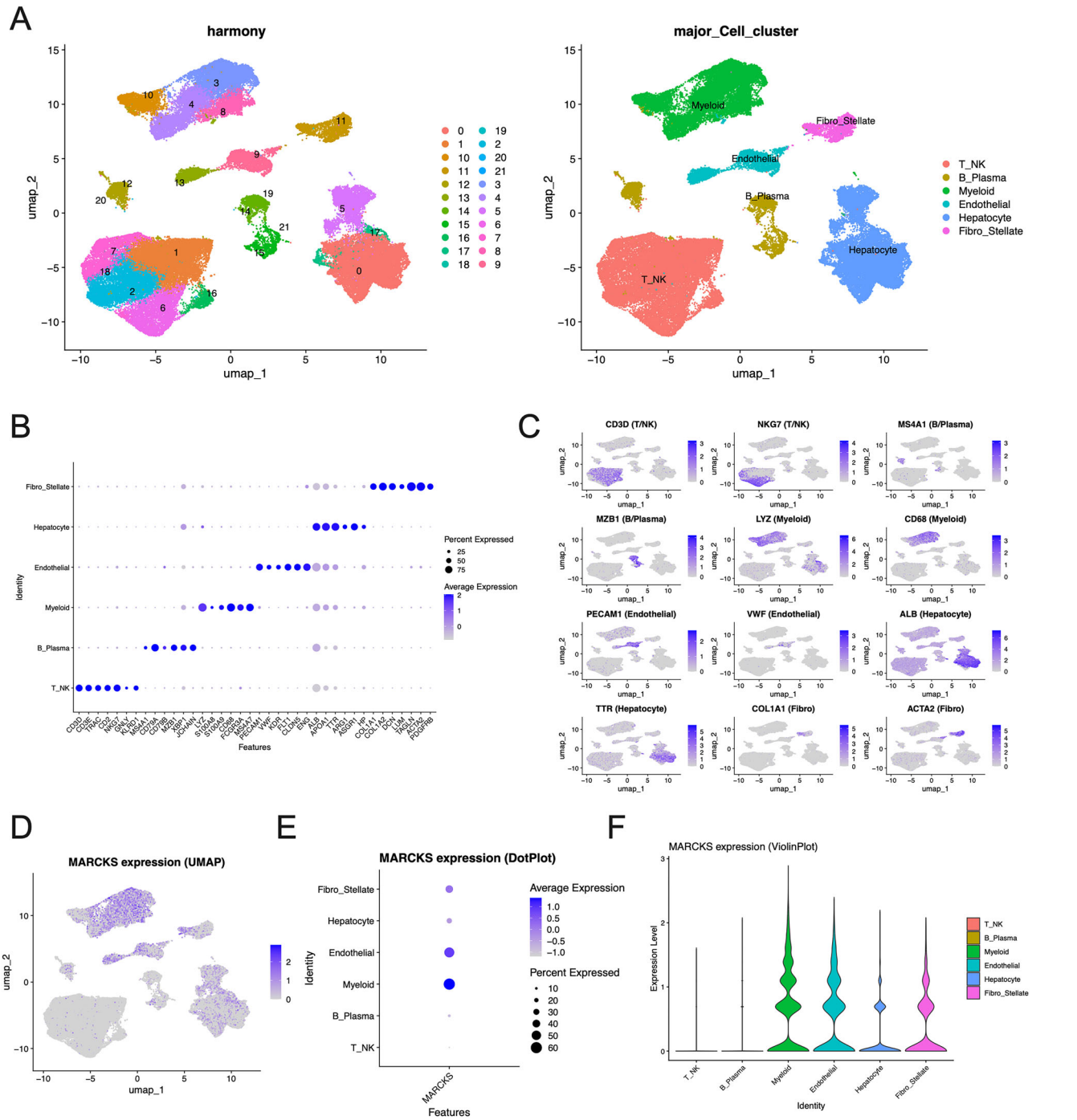

Fig. 4 | Cell clustering and annotation in single-cell transcriptome of HCC (GSE149614). **A** UMAP plots showing unsupervised clustering (left) and annotation of six major lineages: T/NK, B/Plasma, Myeloid, Endothelial, Hepatocyte, and Fibro/Stellate. **B** Dot plots of canonical lineage markers confirming annotation. **C** Feature plots of canonical lineage markers used for annotation. **D** UMAP feature plot showing MARCKS expression. **E** Dot plot of MARCKS expression across six major cell types. **F** Violin plots illustrating distribution and heterogeneity of MARCKS expression among lineages.

progression, MARCKS is closely associated with STAT3-centered immunoregulatory programs and M2-like macrophage polarization, linking tumor-intrinsic signaling states to the establishment of an immunosuppressive tumor immune microenvironment. Through these associations, MARCKS contributes to tumor progression and immune evasion in HCC.

Collectively, our findings position MARCKS as a potential biomarker of immunosuppressive tumor states and a candidate target for therapeutic intervention. While the precise hierarchical relationship between MARCKS and STAT3 signaling warrants further investigation, modulation of MARCKS-associated pathways may represent a rational strategy to remodel the tumor immune microenvironment and improve immunotherapeutic responsiveness in HCC.

Methods

Data acquisition

RNA-seq raw count data, clinical information, and somatic mutation (MAF) files for HCC were downloaded from the TCGA-LIHC cohort via the Genomic Data Commons (GDC; https://portal.gdc.cancer.gov/projects/TCGA-LIHC; dbGaP accession: phs000178). Pan-cancer RNA-seq data integrating TCGA and GTEx samples were obtained from the UCSC Xena

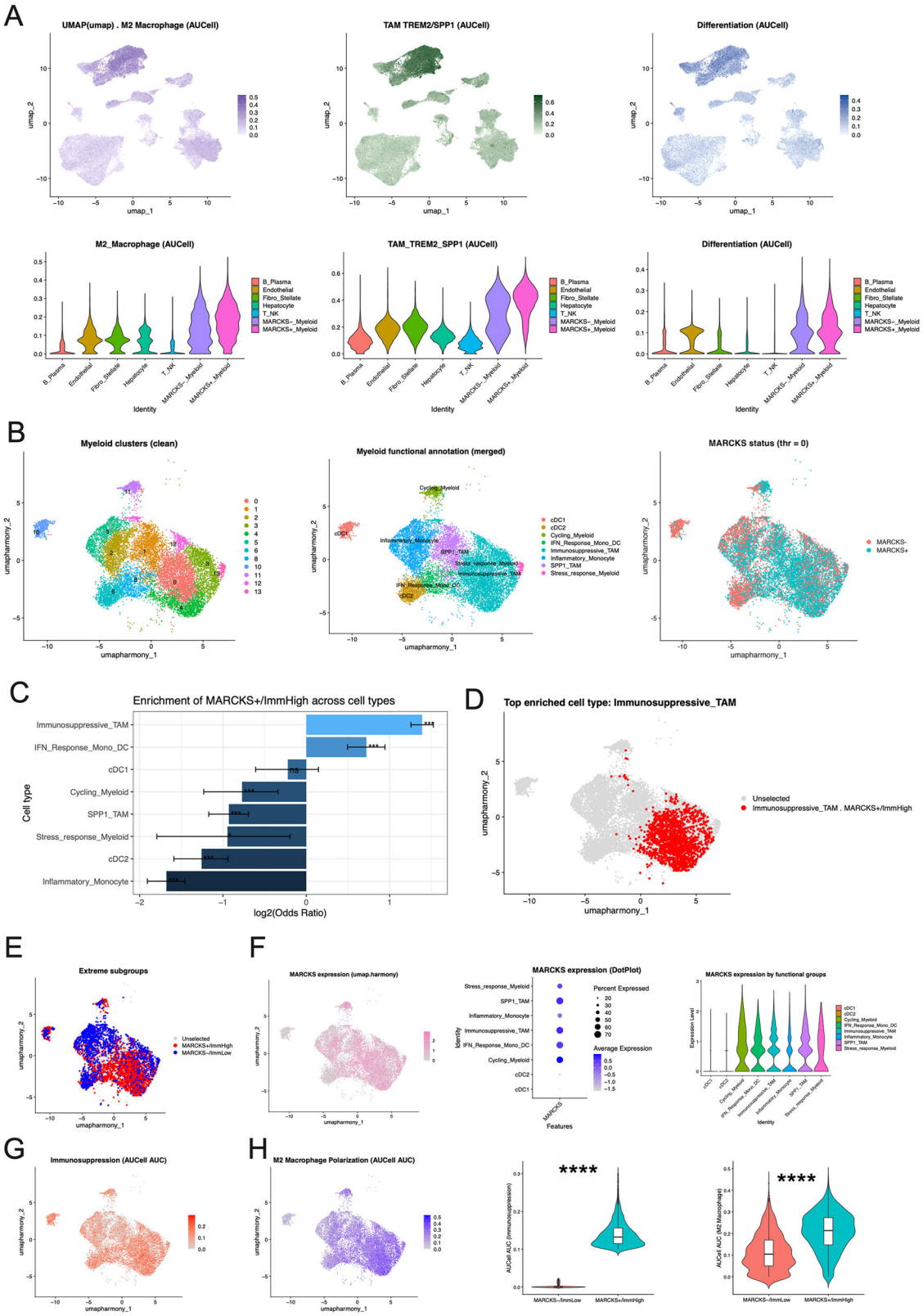

Fig. 5 | MARCKS expression defines immunosuppressive TAMs in the HCC myeloid compartment. A AUCell scoring of functional signatures, including differentiation, proliferation, M2 macrophage polarization, EMT/malignancy, immunosuppression, immune checkpoints, and TAM TREM2/SPP1, stratified by MARCKS status. **B** Reclustering of myeloid cells and functional annotation. **C** Distribution of MARCKS+ versus MARCKS− cells across myeloid functional subsets. **D** UMAP highlighting immunosuppressive TAMs as the top-enriched subtype in MARCKS+ cells. **E** Extreme subgroup analysis comparing MARCKS +/ImmHigh with MARCKS−/ImmLow cells. **F** MARCKS expression across myeloid subsets shown by UMAP, dot plot, and violin plot. **G** AUCell violin plots of immunosuppression scores in MARCKS+ versus MARCKS− cells. **H** AUCell violin plots of M2 polarization scores in MARCKS+ versus MARCKS− cells (Wilcoxon test, **** $p < 0.0001$).

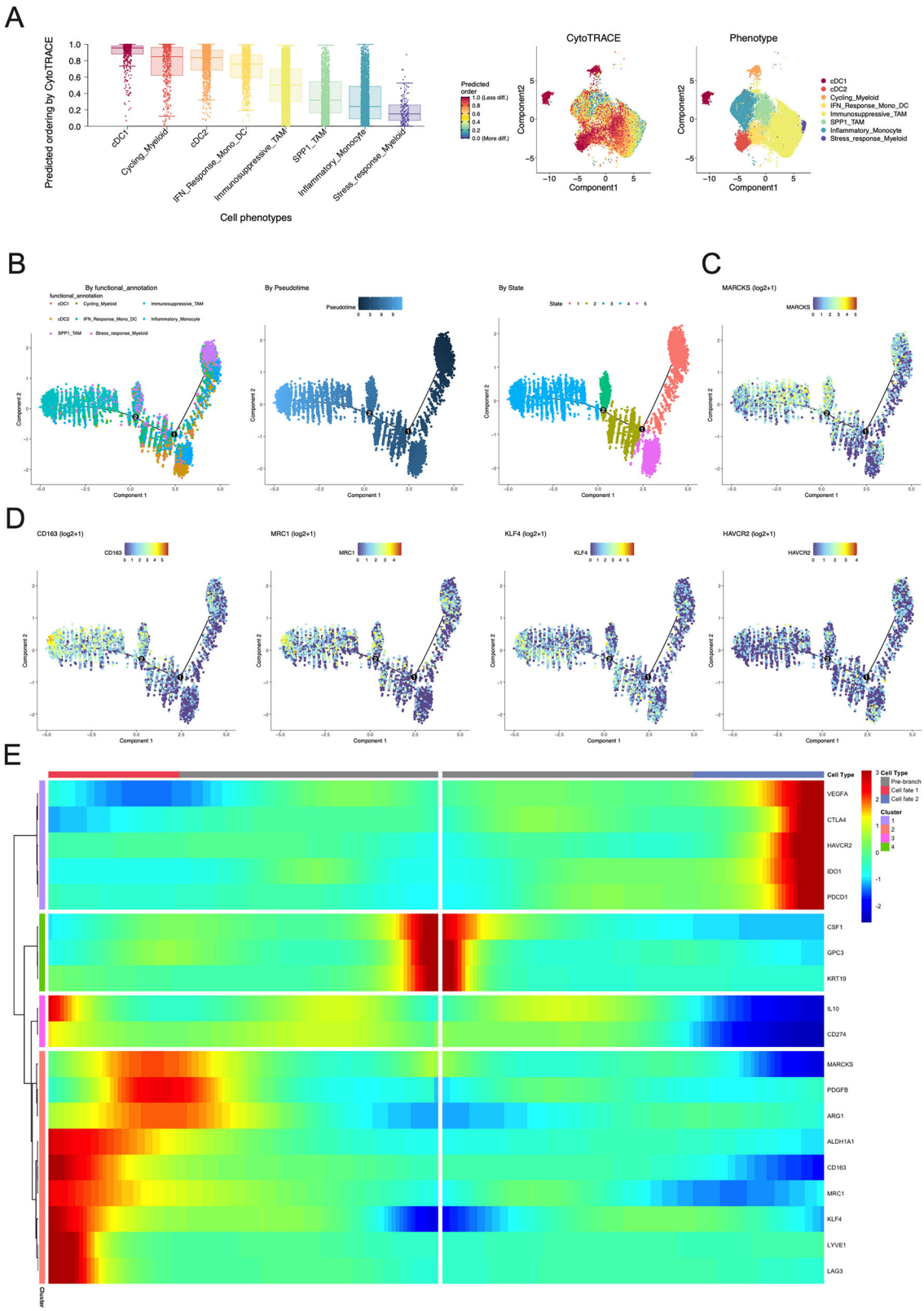

Fig. 6 | CytoTRACE and pseudotime analyses reveal MARCKS-associated immunosuppressive myeloid trajectories. **A** CytoTRACE analysis showing predicted differentiation potential of myeloid subtypes (left), UMAP colored by CytoTRACE score (middle), and functional phenotype annotation (right). **B** Pseudotime trajectories reconstructed by Slingshot and Monocle2, colored by functional annotation, pseudotime, and state. **C** MARCKS expression dynamics along pseudotime trajectory. **D** Expression of representative immunosuppressive/M2-related genes (CD163, MRC1, KLF4, HAVCR2) along trajectories. **E** Heatmap of branched expression dynamics (BEAM analysis) highlighting immunosuppressive and tumor-promoting gene programs (e.g., VEGFA, CTLA4, PDCD1, CSF1, ARG1, MARCKS).

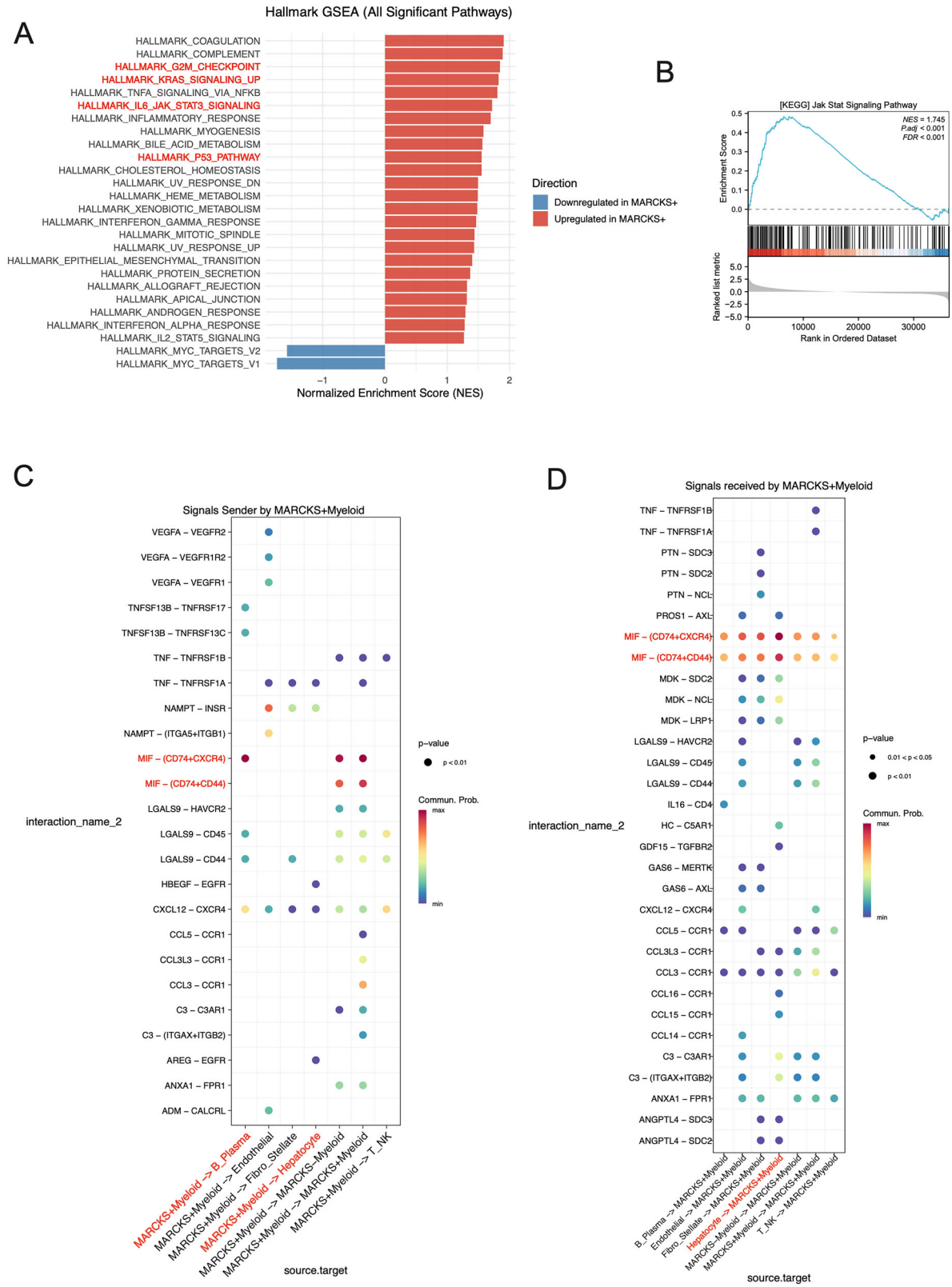

Fig. 7 | Hallmark enrichment and cell–cell communication of MARCKS$^+$ myeloid cells. A Hallmark GSEA of DEGs between MARCKS$^+$ and MARCKS$^-$ myeloid cells showing enrichment of immunosuppressive and inflammatory pathways, including IL6/JAK/STAT3, TNFα/NFκB, and immune checkpoints. **B** KEGG pathway enrichment in TCGA-LIHC confirming upregulation of the JAK–STAT signaling pathway in MARCKS-high tumors. **C** CellChat analysis of ligand–receptor interactions. Left: signals sent by MARCKS$^+$ myeloid cells to other cell types (e.g., VEGFA–VEGFR, TNF–TNFR, LGALS9–HAVCR2, MIF–CD74 + CXCR4/CD44). **D** Signals received by MARCKS$^+$ myeloid cells, indicating bidirectional immunosuppressive signaling.

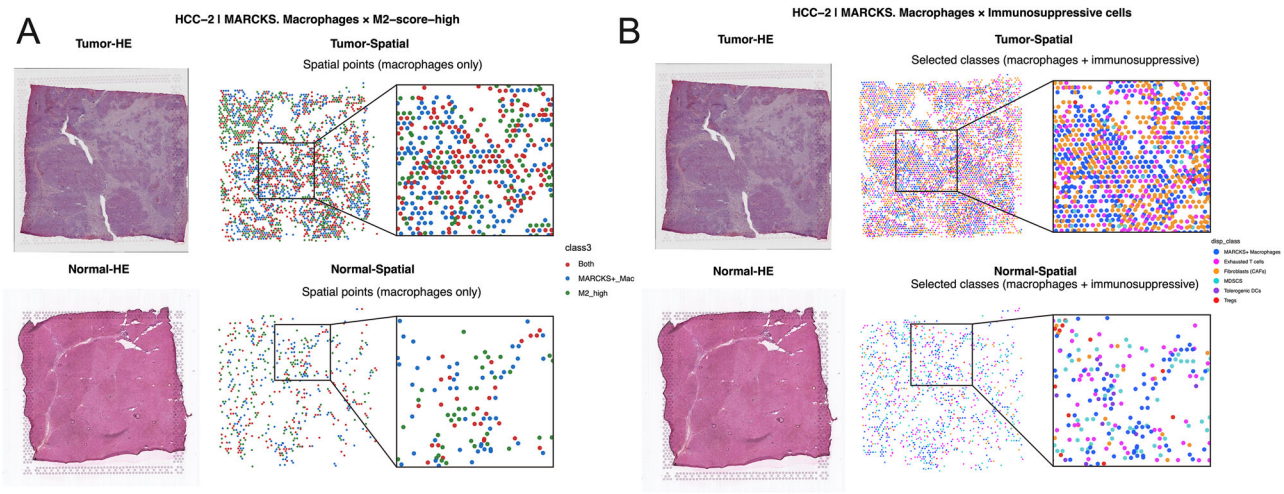

Fig. 8 | Spatial transcriptomics of MARCKS$^+$ macrophages in HCC. A HE-stained image (left) and spatial distribution maps (middle and right) showing colocalization of MARCKS$^+$ macrophages and M2-score-high macrophages in tumor versus adjacent normal tissue of HCC-2I. **B** HE-stained images (left) and spatial maps (middle and right) showing colocalization of MARCKS$^+$ macrophages with immunosuppressive cells, including exhausted T cells, CAFs, MDSCs, tolerogenic DCs, and Tregs, in tumor versus normal regions.

Toil recompute dataset (dataset ID: tcga_RSEM_gene_tpm; release date: 2016-09-01; https://xenabrowser.net/). Single-cell RNA-seq dataset GSE149614 was retrieved from the Gene Expression Omnibus (https://www.ncbi.nlm.nih.gov/geo/query/acc.cgi?acc=GSE149614). Spatial transcriptomics dataset HRA000437 was acquired from the National Genomics Data Center (NGDC; https://ngdc.cncb.ac.cn/gsa-human/browse/HRA000437).

All datasets were publicly available, and no additional ethical approval was required.

Bulk RNA-seq analyses

TCGA-LIHC RNA-seq data were downloaded as raw count matrices from the Genomic Data Commons. For downstream analyses, raw counts were normalized to TPM values and subsequently transformed using log2(TPM + 1). Only primary tumor samples with complete clinical and mutation information were retained. Genes with undetectable expression (TPM = 0) in more than 50% of tumor samples were filtered out to ensure statistical robustness.

Patients were dichotomized into MARCKS-high and MARCKS-low groups using the median MARCKS expression level as the cutoff. Differentially expressed genes (DEGs) between the two groups were identified using limma (v3.58.1), with $|\log2FC| > 1$ and FDR < 0.05. Functional enrichment of Hallmark and KEGG pathways was performed using clusterProfiler (v4.10.0).

Immune infiltration was estimated using xCell implemented in immunedeconv (v3.0.0).

Associations between MARCKS expression and immune cell scores, immune checkpoint molecules, immunosuppressive mediators, and macrophage polarization markers were assessed using Spearman correlation, consistent with the non-normal distribution of TPM expression values. Correlation networks were visualized using igraph and corrplot.

For survival analyses, overall survival (OS)/disease-specific Survival(DSS)/progression-free Interval(PFI) were compared between MARCKS-high and MARCKS-low groups using Kaplan–Meier curves and the log-rank test. Hazard ratios (HRs) and 95% confidence intervals (CIs) were estimated using univariable and multivariable Cox proportional hazards models (survival v3.5). The proportional hazards assumption was tested using Schoenfeld residuals (cox.zph()).

Somatic mutation profiles were processed with maftools (v2.18.0). Differential mutation frequencies were evaluated using Fisher's exact test. Tumor mutation burden (TMB) was calculated as the total number of nonsynonymous mutations per megabase.

Single-cell RNA-seq analyses (GSE149614)

Single-cell transcriptomic data from GSE149614 were processed using Seurat. Raw count matrices were imported to create a Seurat object, and standard quality-control metrics were computed, including the number of detected genes (nFeature_RNA), UMI counts (nCount_RNA), and the percentage of mitochondrial transcripts (percent.mt; defined using genes starting with "MT-"). Cells were retained if they expressed 200–6000 genes, had nCount_RNA < 40,000, and exhibited <20% mitochondrial reads.

Normalization and variance stabilization were performed using SCTransform (vst.flavor = "v2"). Principal component analysis (PCA) was conducted to obtain 50 principal components, and batch effects across samples (orig.ident) were corrected using Harmony based on the first 30 PCs. The Harmony-corrected embeddings were used for constructing the shared nearest-neighbor graph, followed by Louvain clustering at a resolution of 0.5. Two-dimensional embeddings were generated using UMAP and t-SNE, also based on the Harmony reduction (dims 1–30).

Major cell lineages were annotated using canonical markers, including T/NK (CD3D, NKG7), B/Plasma (MS4A1, MZB1), Myeloid (LYZ, CD68), Endothelial (PECAM1, VWF), Hepatocytes (ALB, TTR), and Fibro/Stellate cells (COL1A1, ACTA2). (The markers for cell annotation are listed in Supplementary Table 2).

For myeloid-focused analyses, myeloid cells were extracted and reclustered to identify functional subsets, such as immunosuppressive TAMs, SPP1$^+$ TAMs, dendritic cells, and monocytes. Gene set activity related to M2 polarization, differentiation, and immunosuppression was quantified using AUCell. Differentiation potential was inferred using CytoTRACE, and developmental trajectories were reconstructed using Slingshot and Monocle2 (DDRTree), including branched expression analysis (BEAM) for dynamic gene programs. Hallmark pathway enrichment in MARCKS$^+$ versus MARCKS$^-$ myeloid subsets was assessed using fgsea.

Myeloid subset analysis

The myeloid compartment was extracted and reclustered using Seurat. Subclusters were annotated into functional states, including immunosuppressive TAMs, SPP1$^+$ TAMs, stress-response myeloid cells, dendritic cells, and monocytes. Gene set activity was quantified with AUCell (v1.22.0) using curated signatures related to differentiation, M2 polarization, and immunosuppression (full gene lists provided in Supplementary Table S3). Differentiation potential was inferred using CytoTRACE (v0.3.3). Pseudotime trajectories were reconstructed with Slingshot (v2.10.0) and Monocle2

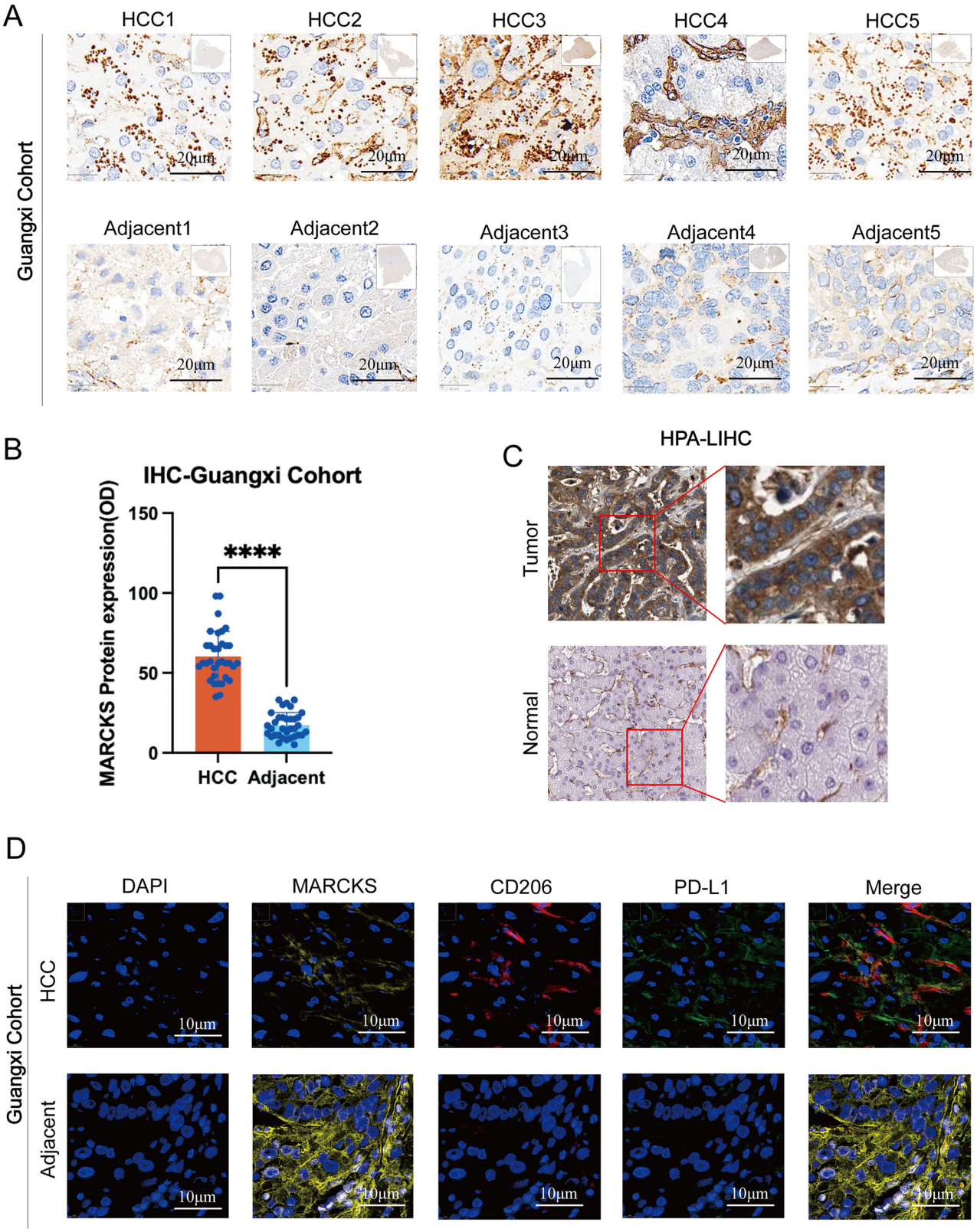

Fig. 9 | MARCKS expression in HCC tissues. A Representative IHC staining of MARCKS in Guangxi cohort HCC and adjacent tissues. **B** Quantification of MARCKS protein expression in HCC versus adjacent tissues. **C** IHC validation of MARCKS expression from the HPA database. **D** Multiplex immunofluorescence staining showing co-localization of MARCKS, CD206, and PD-L1 in HCC tissues.

(v2.28.0), with DDRTree for dimensionality reduction and BEAM for branched gene expression analysis. Gene set enrichment analysis (GSEA) was performed with fgsea (v1.26.0) using MSigDB Hallmark pathways. Pathways with adjusted $p < 0.20$ were considered significant.

Cell–cell communication and spatial transcriptomics

Cell–cell communication networks were inferred using CellChat (v1.5.0). A maximum of 3000 cells per lineage was sampled to reduce computational burden. MARCKS^{+} myeloid cell interactions were evaluated using the

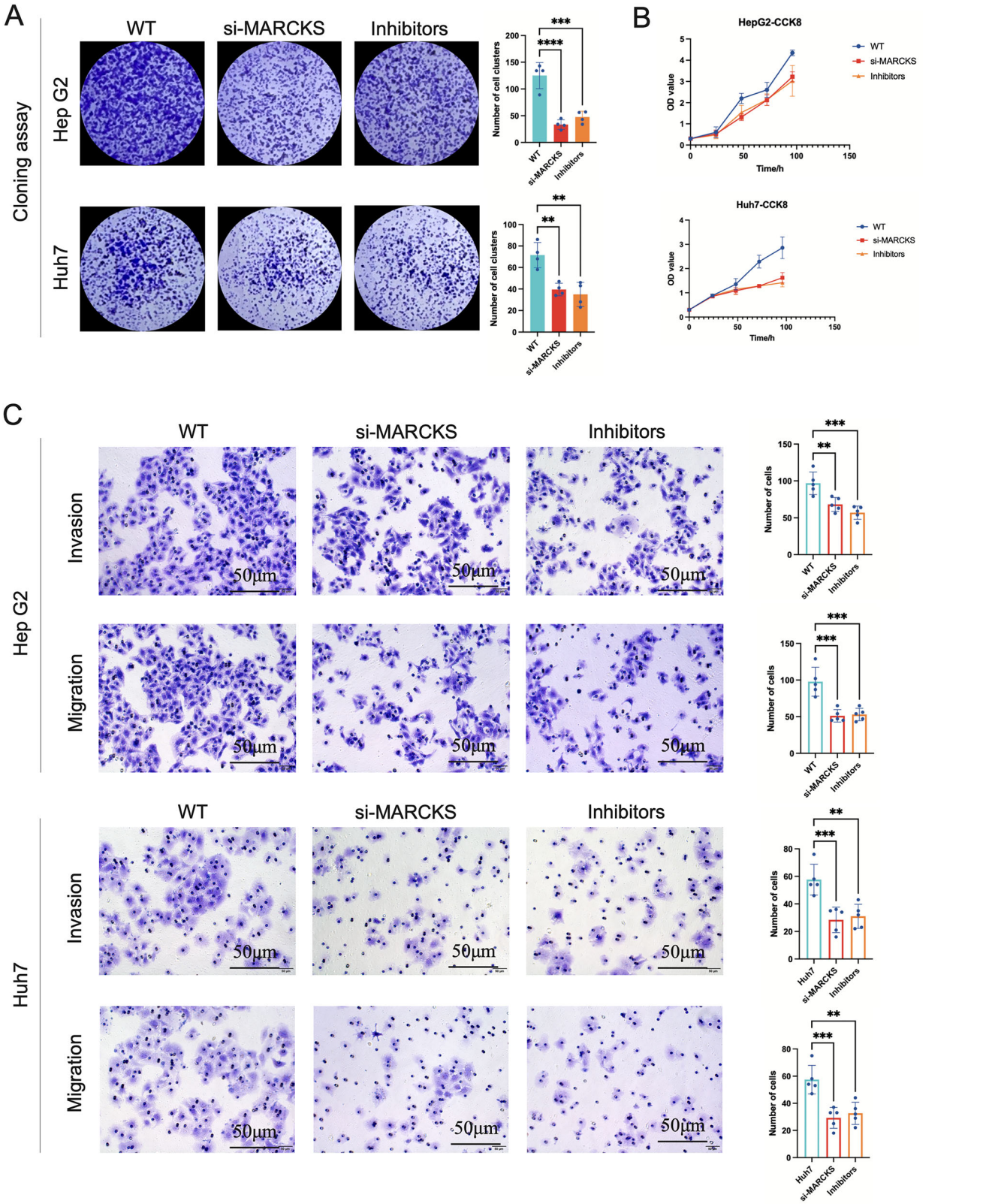

Fig. 10 | MARCKS promotes proliferation, migration, and invasion in HCC cells. A Colony formation assays in HepG2 and Huh7 cells with WT, si-MARCKS, or Stattic treatment. **B** CCK-8 proliferation curves under the indicated conditions. **C** Transwell migration and invasion assays in HepG2 and Huh7 cells.

CellChatDB.human database. For spatial transcriptomics, data from NGDC were processed with Seurat and customized pipelines. MARCKS^{+} macrophages were identified and colocalized with M2 and immunosuppressive signatures in tumor regions.

In vitro assays

Human HCC cell lines HepG2 and Huh7 (ATCC) were cultured in DMEM (Gibco) supplemented with 10% fetal bovine serum (FBS; Gibco) and 1% penicillin/streptomycin (Gibco) at 37 °C in a humidified atmosphere with

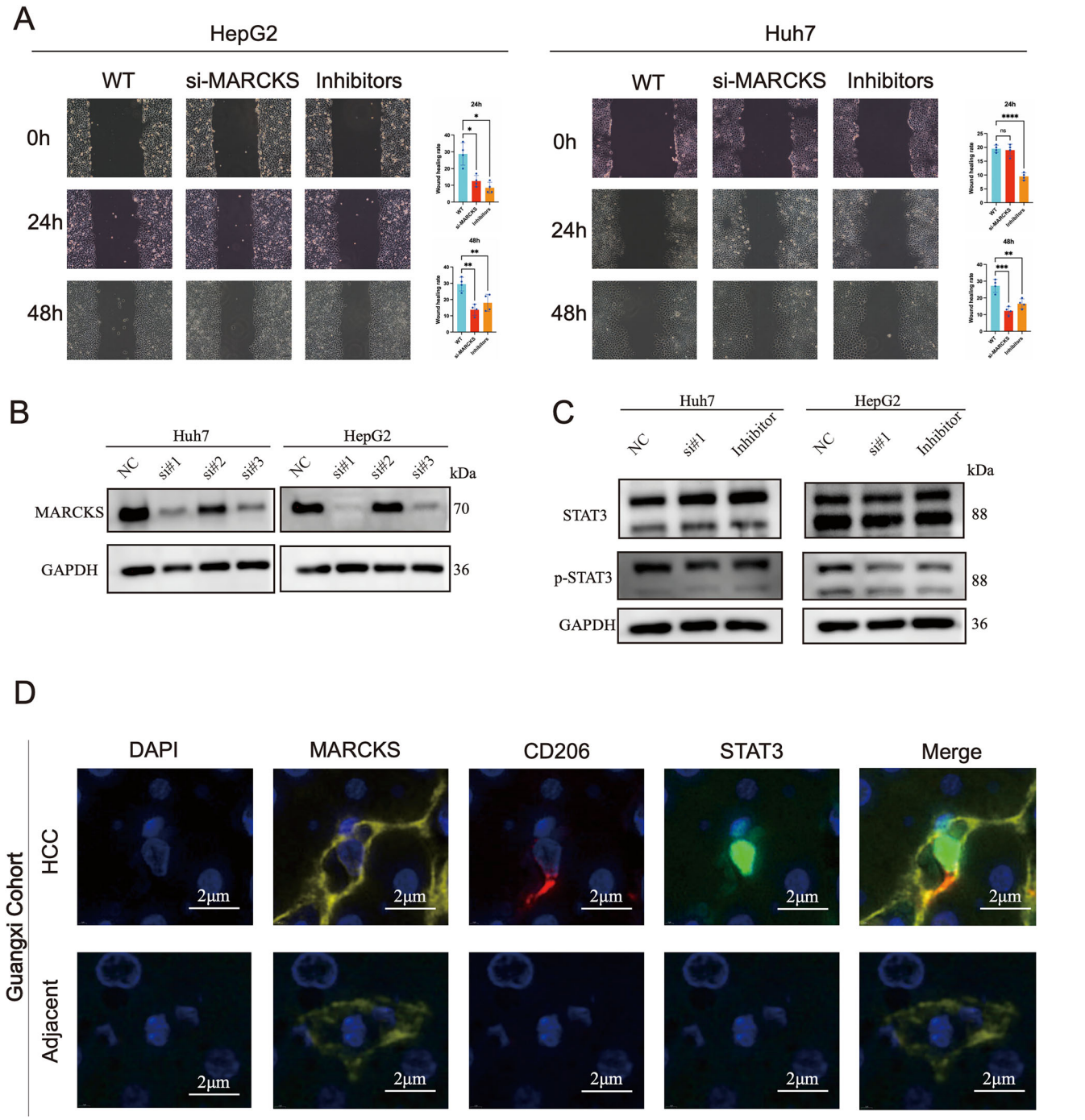

Fig. 11 | MARCKS activates STAT3 signaling in HCC cells. A Wound-healing assays showing delayed closure after MARCKS knockdown or Stattic treatment. **B** Western blot validation of MARCKS knockdown efficiency. **C** Western blot showing reduced STAT3 phosphorylation with MARCKS knockdown or inhibition. **D** Immunofluorescence staining confirming co-localization of MARCKS, CD206, and STAT3 in HCC tissues.

5% CO_2. MARCKS knockdown was performed using siRNAs (GenePharma, Shanghai; sequences listed in Supplementary Table S5) transfected with Lipofectamine 3000 (Thermo Fisher). Stattic (MCE,CAS 19983-44-9) was used as a STAT3 inhibitor at 5 μM for 24–48 h.

Functional assays

For colony formation assays, 500 cells were seeded per well in 6-well plates, cultured for 10–14 days, fixed with 4% paraformaldehyde (Beyotime), and stained with 0.1% crystal violet (Beyotime). Colonies containing more than 50 cells were counted. Cell proliferation was assessed using the CCK-8 kit (Dojindo) with absorbance measured at 450 nm. Migration and invasion assays were performed with 8-μm pore size transwell chambers (Corning) with or without Matrigel (BD Biosciences). Cells (3×10^4) were seeded in serum-free medium in the upper chamber; after 24–48 h, migrated or invaded cells were fixed, stained, and counted. Wound-healing assays were performed by scratching confluent monolayers with sterile 200-μL pipette tips, and images were captured at 0, 24, and 48 h.

Protein and tissue analyses

Whole-cell lysates were prepared with RIPA buffer(Beyotime) containing protease/phosphatase inhibitors (Roche). Proteins were separated by

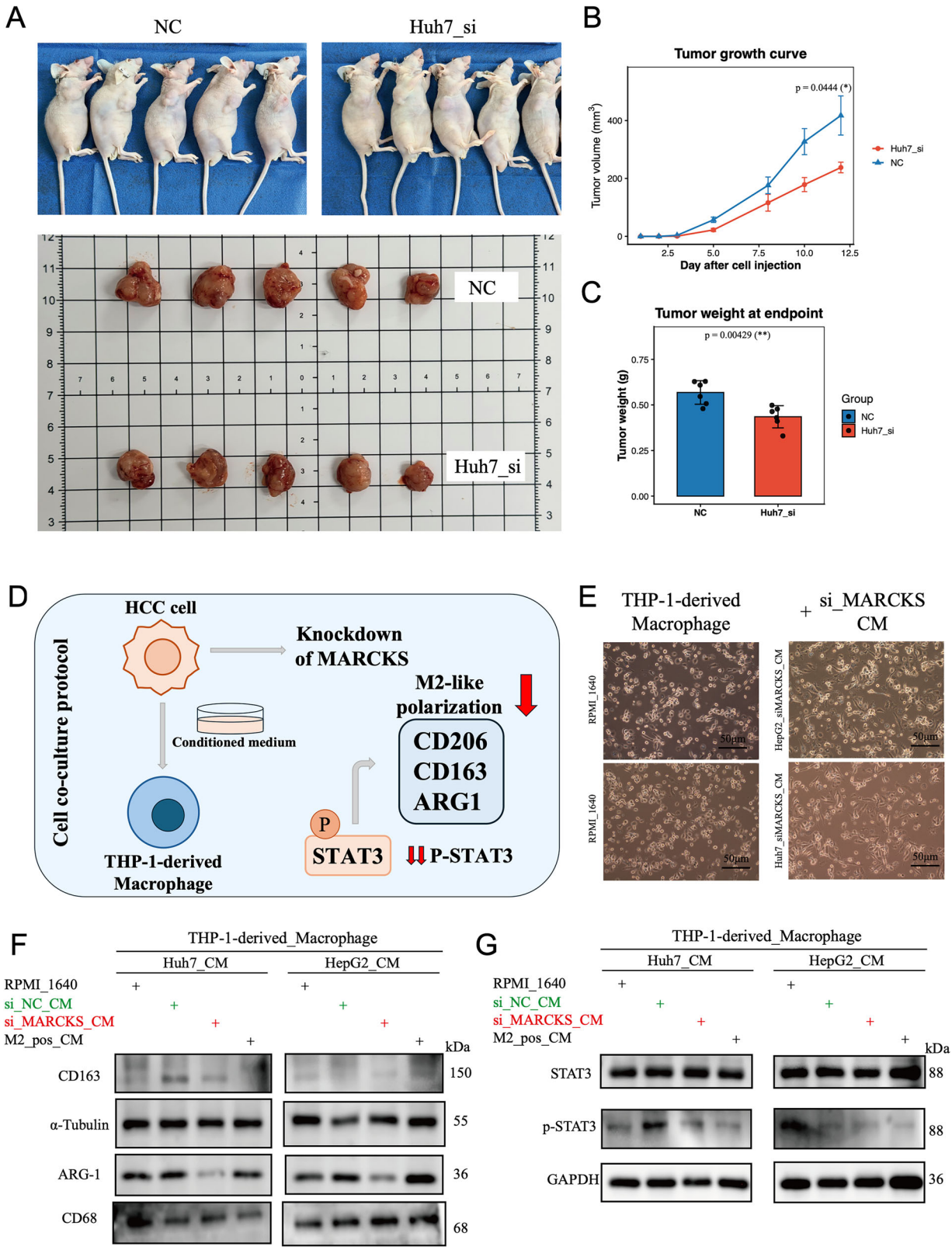

Fig. 12 | MARCKS knockdown suppresses tumor growth in vivo and attenuates macrophage M2-like polarization. A Representative images of subcutaneous xenograft tumors derived from Huh7 cells transfected with control or MARCKS-targeting siRNA. **B** Tumor growth curves showing tumor volume measured at indicated time points. Tumor volume was calculated as (length × width^2) /2. **C** Tumor weights at the experimental endpoint ($n = 5$ mice per group). **D** Schematic illustration of the conditioned medium (CM)-based co-culture system. **E** Representative phase-contrast images of THP-1-derived macrophages treated with conditioned media from control or MARCKS-silenced HCC cells (scale bar = 50 μm). **F** Western blot analysis of M2-associated markers (CD163 and ARG1) and CD68 in THP-1–derived macrophages. **G** Western blot analysis of phosphorylated STAT3 (p-STAT3) and total STAT3 following CM stimulation. Data are representative of at least three independent experiments. $P < 0.05$ was considered statistically significant.

SDS-PAGE and transferred to PVDF membranes. The following antibodies were used: MARCKS (Proteintech, Cat No. 10004-2-Ig,1:1000), STAT3 (Proteintech, Cat No. 10253-2-AP,1:1000), p-STAT3 (Proteintech, Cat No. 60199-1-Ig, 1:1000), and GAPDH (Proteintech, Cat No. 60004-1-Ig,1:5000). For immunohistochemistry (IHC), paraffin-embedded tumor and adjacent tissues from the Guangxi cohort (The Ethics Committee of the First Affiliated Hospital of Guangxi Medical University has approved this study, and specimen collection was conducted according to the principles outlined in the Declaration of Helsinki. Certificate Number: 2024-E144-01,2025-E0874. Each patient provided written informed consent.) were stained with anti-MARCKS and quantified by ImageJ. For immunofluorescence (IF), tissues were stained with antibodies against CD206 (Proteintech, Cat No. 18704-1-AP,1:200), and STAT3 (CST, 1:200). Secondary antibodies included Alexa Fluor 488/594 conjugates (Invitrogen). Nuclei were counterstained with DAPI (Sigma), and images were acquired on a Leica SP8 confocal microscope.

Subcutaneous xenograft assay

Male BALB/c nude mice were maintained under specific pathogen-free conditions. Huh7 hepatocellular carcinoma cells were transfected with control siRNA or MARCKS-targeting siRNA, harvested, washed with PBS, and subcutaneously injected into the flanks of nude mice. Tumor length and width were measured at regular intervals using calipers, and tumor volume was calculated according to the formula volume = (length × width^2)/2. At the experimental endpoint, mice were sacrificed, and tumors were excised intact, photographed, and weighed for subsequent analyses. All animal procedures were conducted in accordance with institutional guidelines and were approved by the Ethics Committee of the First Affiliated Hospital of Guangxi Medical University (Approval No. 2025-D0499).

Conditioned medium-based macrophage co-culture assay

Huh7 and HepG2 hepatocellular carcinoma cells were transiently transfected with control siRNA or MARCKS-targeting siRNA according to the manufacturer's instructions. Twenty-four hours after transfection, the culture medium was replaced with fresh complete medium, and cells were incubated for an additional 24 h. Conditioned media were then collected, centrifuged at 1000 × *g* for 5 min to remove cellular debris, and used immediately for subsequent experiments.

THP-1 monocytes were differentiated into M0 macrophages by treatment with phorbol 12-myristate 13-acetate (PMA, 100 ng/ml) for 48 h. After differentiation, macrophages were washed with PBS and incubated with conditioned media derived from HCC cells for 48 h. RPMI 1640 medium served as a negative control, and M2-polarizing medium was used as a positive control where indicated.

Following co-culture, macrophages were harvested for protein extraction and Western blot analysis. Representative morphological changes were documented using microscopy. All experiments were independently repeated at least three times.

Statistical analyses

All analyses were performed in R (v4.5.0). Comparisons between two groups were conducted using Student's *t* test or Mann–Whitney *U* test, while multiple groups were compared by ANOVA or Kruskal–Wallis test. Correlations were analyzed with Pearson's or Spearman's method. Survival analyses were performed using Kaplan–Meier with log-rank test and Cox regression. *p*-values < 0.05 were considered statistically significant (ns, $p > 0.05$; $^{*}p < 0.05$; $^{**}p < 0.01$; $^{***}p < 0.001$; $^{****}p < 0.0001$).

All abbreviations used in this study are listed in Supplementary Table S6.

Data availability

RNA-seq raw count data, clinical information, and somatic mutation (MAF) files for HCC were obtained from the TCGA-LIHC cohort via the Genomic Data Commons (https://portal.gdc.cancer.gov/projects/TCGA-LIHC; dbGaP: phs000178). Pan-cancer RNA-seq data integrating TCGA and GTEx were retrieved from the UCSC Xena Toil recompute dataset (https://xenabrowser.net/). The single-cell RNA-seq dataset GSE149614 was downloaded from GEO (https://www.ncbi.nlm.nih.gov/geo/query/acc.cgi?acc=GSE149614), and the spatial transcriptomics dataset HRA000437 was obtained from NGDC (https://ngdc.cncb.ac.cn/gsa-human/browse/HRA000437).

Code availability

The custom scripts and codes used for data processing and analysis are available from the corresponding author upon reasonable request.

Received: 17 October 2025; Accepted: 2 March 2026;
Published online: 11 March 2026

References

1. Bray, F. et al. Global cancer statistics 2022: GLOBOCAN estimates of incidence and mortality worldwide for 36 cancers in 185 countries. *CA Cancer J. Clin.* **74**, 229–263 (2024).
2. Llovet, J. M. et al. Locoregional therapies in the era of molecular and immune treatments for hepatocellular carcinoma. *Nat. Rev. Gastroenterol. Hepatol.* **18**, 293–313 (2021).
3. Sonbol, M. B. et al. Systemic therapy and sequencing options in advanced hepatocellular carcinoma: a systematic review and network meta-analysis. *JAMA Oncol.* **6**, e204930 (2020).
4. Vogel, A. & Martinelli, E. ESMO Guidelines Committee. Updated treatment recommendations for hepatocellular carcinoma (HCC) from the ESMO Clinical Practice Guidelines. *Ann. Oncol.* **32**, 801–805 (2021).
5. He, H. et al. Multi-dimensional single-cell characterization revealed suppressive immune microenvironment in AFP-positive hepatocellular carcinoma. *Cell Discov.* **9**, 60 (2023).
6. Wang, Y. F. et al. Spatial maps of hepatocellular carcinoma transcriptomes reveal spatial expression patterns in tumor immune microenvironment. *Theranostics* **12**, 4163–4180 (2022).
7. Chen, S. et al. Distinct single-cell immune ecosystems distinguish true and de novo HBV-related hepatocellular carcinoma recurrences. *Gut* **72**, 1196–1210 (2023).
8. Shen, H. et al. Prognostic biomarker MITD1 and its correlation with immune infiltrates in hepatocellular carcinoma (HCC). *Int. Immunopharmacol.* **81**, 106222 (2020).
9. Xiang, X., Wang, J., Lu, D. & Xu, X. Targeting tumor-associated macrophages to synergize tumor immunotherapy. *Signal Transduct. Target. Ther.* **6**, 75 (2021).
10. Chen, D., Zhang, X., Li, Z. & Zhu, B. Metabolic regulatory crosstalk between tumor microenvironment and tumor-associated macrophages. *Theranostics* **11**, 1016–1030 (2021).
11. Chu, X., Tian, Y. & Lv, C. Decoding the spatiotemporal heterogeneity of tumor-associated macrophages. *Mol. Cancer* **23**, 150 (2024).
12. Li, C. et al. Tumor-associated macrophages: potential therapeutic strategies and future prospects in cancer. *J. Immunother. Cancer* **9**, e001341 (2021).
13. Qian, J., Li, J., Ma, H. & Ji, W. Exosomal circ-ADRM1 promotes lung adenocarcinoma progression and induces macrophage M2 polarization through regulating MMP14 mRNA and protein. *Anticancer Drugs* **34**, 333–343 (2023).
14. Ruf, B. et al. Tumor-associated macrophages trigger MAIT cell dysfunction at the HCC invasive margin. *Cell* **186**, 3686–3705.e32 (2023).
15. Cheng, K. et al. Tumor-associated macrophages in liver cancer: from mechanisms to therapy. *Cancer Commun.* **42**, 1112–1140 (2022).
16. El Amri, M., Fitzgerald, U. & Schlosser, G. MARCKS and MARCKS-like proteins in development and regeneration. *J. Biomed. Sci.* **25**, 43 (2018).

17. Chen, Z. et al. The myristoylated alanine-rich C-kinase substrates (MARCKS): a membrane-anchored mediator of the cell function. *Autoimmun. Rev.* **20**, 102942 (2021).
18. Beckmann, L. et al. MARCKS affects cell motility and response to BTK inhibitors in CLL. *Blood* **138**, 544–556 (2021).
19. Bickeböller, M. et al. Functional characterization of the tumor-suppressor MARCKS in colorectal cancer and its association with survival. *Oncogene* **34**, 1150–1159 (2015).
20. Huang, X. Z. et al. Single-cell sequencing of ascites fluid illustrates heterogeneity and therapy-induced evolution during gastric cancer peritoneal metastasis. *Nat. Commun.* **14**, 822 (2023).
21. Zhang, L. et al. MARCKS inhibition cooperates with autophagy antagonists to potentiate the effect of standard therapy against drug-resistant multiple myeloma. *Cancer Lett.* **480**, 29–38 (2020).
22. Reddy, S. P., Natarajan, V. & Dudek, A. Z. MARCKS is marked in combating lung cancer growth and acquired resistance. *Am. J. Respir. Crit. Care Med.* **190**, 1084–1086 (2014).
23. Chen, C. H. et al. Upregulation of MARCKS in kidney cancer and its potential as a therapeutic target. *Oncogene* **36**, 3588–3598 (2017).
24. Naboulsi, W. et al. Quantitative tissue proteomics analysis reveals versican as potential biomarker for early-stage hepatocellular carcinoma. *J. Proteome Res.* **15**, 38–47 (2016).
25. Masaki, T. et al. Comparison study of the expressions of myristoylated alanine-rich C kinase substrate in hepatocellular carcinoma, liver cirrhosis, chronic hepatitis, and normal liver. *Int. J. Oncol.* **26**, 661–671 (2005).
26. Lu, H. et al. MARCKS is a new prognostic biomarker in hepatocellular carcinoma. *Int. J. Gen. Med.* **16**, 1603–1619 (2023).
27. Ren, X. et al. MARCKS on tumor-associated macrophages is correlated with immune infiltrates and poor prognosis in hepatocellular carcinoma. *Cancer Invest* **39**, 756–768 (2021).
28. Vogel, A., Meyer, T., Sapisochin, G., Salem, R. & Saborowski, A. Hepatocellular carcinoma. *Lancet* **400**, 1345–1362 (2022).
29. Donne, R. & Lujambio, A. The liver cancer immune microenvironment: therapeutic implications for hepatocellular carcinoma. *Hepatology* **77**, 1773–1796 (2023).
30. Rimassa, L., Finn, R. S. & Sangro, B. Combination immunotherapy for hepatocellular carcinoma. *J. Hepatol.* **79**, 506–515 (2023).
31. Greten, T. F. et al. Biomarkers for immunotherapy of hepatocellular carcinoma. *Nat. Rev. Clin. Oncol.* **20**, 780–798 (2023).
32. Wang, Z., Wang, Y., Gao, P. & Ding, J. Immune checkpoint inhibitor resistance in hepatocellular carcinoma. *Cancer Lett.* **555**, 216038 (2023).
33. Gao, J., Wang, W. Q., Pei, Q., Lord, M. S. & Yu, H. J. Engineering nanomedicines through boosting immunogenic cell death for improved cancer immunotherapy. *Acta Pharm. Sin.* **41**, 986–994 (2020).
34. Pitt, J. M. et al. Targeting the tumor microenvironment: removing obstruction to anticancer immune responses and immunotherapy. *Ann. Oncol.* **27**, 1482–1492 (2016).
35. Mellman, I., Chen, D. S., Powles, T. & Turley, S. J. The cancer-immunity cycle: indication, genotype, and immunotype. *Immunity* **56**, 2188–2205 (2023).
36. Ren, X. et al. Insights gained from single-cell analysis of immune cells in the tumor microenvironment. *Annu. Rev. Immunol.* **39**, 583–609 (2021).
37. Fu, T. et al. Spatial architecture of the immune microenvironment orchestrates tumor immunity and therapeutic response. *J. Hematol. Oncol* **14**, 98 (2021).
38. Wu, J. et al. A noninvasive approach to evaluate tumor immune microenvironment and predict outcomes in hepatocellular carcinoma. *Phenomics* **3**, 549–564 (2023).
39. Shao, K. et al. Copper transporter gene ATP7A: a predictive biomarker for immunotherapy and targeted therapy in hepatocellular carcinoma. *Int. Immunopharmacol.* **114**, 109518 (2023).
40. Li, Y. et al. CircTRIM1 encodes TRIM1-269aa to promote chemoresistance and metastasis of TNBC via enhancing CaM-dependent MARCKS translocation and PI3K/AKT/mTOR activation. *Mol. Cancer* **23**, 102 (2024).
41. Yang, Y. et al. Targeting phospho-MARCKS overcomes drug resistance and induces antitumor activity in preclinical models of multiple myeloma. *Leukemia* **29**, 715–726 (2015).
42. Niewerth, D. et al. Molecular basis of resistance to proteasome inhibitors in hematological malignancies. *Drug Resist. Updates* **18**, 18–35 (2015).
43. Jarboe, J. S. et al. MARCKS regulates growth and radiation sensitivity and is a novel prognostic factor for glioma. *Clin. Cancer Res. J. Am. Assoc. Cancer Res.* **18**, 3030–3041 (2012).

Acknowledgements

This work was supported by the Guangxi Science and Technology Base and Talent Special Fund (AB23026002); the National Natural Science Foundation of China (No. 82360465, 82560579); the Guangxi Natural Science Foundation (No. 2024GXNSFDA010029, 2025GXNSFAA069704, 2026GXNSFBA00640315); the Guangxi Key Laboratory of Longevity Science and Technology (Open Fund Project No. gxkllst-20241003); the Guangxi Science and Technology Program (No. AD25069077); the Special Fund for Clinical Discipline Construction of Guangxi Medical University (No. GXMULJZ202402); the Innovation Project of Guangxi Graduate Education (No. YCSW2025252); the Guangxi Natural Science Foundation Youth Science Fund Project (No. 2025GXNSFBA069037); the Young and Middle-aged Scientific Research Capacity Enhancement Project (No. 2024KY0128); the National Postdoctoral Researcher Funding Program (No. GZC20230583); the Open Project of Guangxi Key Laboratory of Enhanced Recovery after Surgery for Gastrointestinal Cancer (No. GXEKL202401); and the Youth Science Foundation of Guangxi Medical University (No. GXMUYSF202501).

Author contributions

Haifei Qin, Qinchen Lu, and Baicheng Hu contributed equally to this work. Haifei Qin, Qinchen Lu, and Baicheng Hu designed and performed most of the experiments and analyses. Chenlu Lan, Honglong Lu, Donghua Gao, Chongjiu Qin, and Kai Peng assisted with data collection, bioinformatics analysis, and figure preparation. Xin Zhou, Yongguang Wei, Xiwen Liao, and Tao Peng provided technical support and contributed to data interpretation. Tao Peng, Liming Shang, and Guangzhi Zhu supervised the project, critically revised the manuscript for important intellectual content, and served as corresponding authors. All authors read and approved the final manuscript.

Competing interests

The authors declare no competing interests.

Additional information

Supplementary information The online version contains supplementary material available at https://doi.org/10.1038/s41698-026-01372-7.

Correspondence and requests for materials should be addressed to Tao Peng, Liming Shang or Guangzhi Zhu.